

# Statistical theory of thermal instability

Andrei F. Illarionov<sup>1</sup> and Igor V. Igumenshchev<sup>2,3</sup>

<sup>1</sup>*P. N. Lebedev Physical Institute, 84/32 Profsoyuznaya Street, Moscow, 117810, Russia*

<sup>2</sup>*Department of Astronomy & Astrophysics, Göteborg University and Chalmers University of Technology, 412 96 Göteborg, Sweden*

<sup>3</sup>*Institute of Astronomy, 48 Pyatnitskaya Street, Moscow, 109117, Russia*

Accepted 1997 September 00. Received 1997 September 00; in original form 1997 September 00

## ABSTRACT

A new statistical approach is presented to study the process of the thermal instability of optically thin unmagnetized plasma. In the frame of this approach the time evolution of mass distribution function over temperature  $\varphi(T)$  is calculated. Function  $\varphi(T)$  characterizes the statistical properties of the multiphase medium of arbitrarily spaced *three-dimensional* structure of arbitrary (small or large) temperature perturbations. We construct our theory under the isobarical condition ( $P = \text{const}$  over space), which is satisfied in the short wavelength limit of the perturbations. The developed theory is illustrated in the case of thermal instability of a slowly expanding interstellar cloud (smooth scenario). Numerical solutions of equations of the statistical theory are constructed and compared with hydrodynamical solutions. The results of both approaches are identical in the short wavelength range when the isobarity condition is satisfied. Also the limits of applicability of the statistical theory are estimated. The possible evolution of initial spectrum of perturbations is discussed. The proposed theory and numerical models can be relevant to the formation of the two-phases medium in the  $\sim 1\text{pc}$  region around quasars. Then small warm ( $T \simeq 10^4\text{K}$ ) clouds are formed as the result of thermal instability in an expanded gas fragment, which is a product of either the star-star or star-accretion disc collision.

**Key words:** hydrodynamics — instabilities — ISM: general — plasmas.

## 1 INTRODUCTION

The interstellar and intergalactic optically thin plasma may be in a variety of thermal phases, depending on local heating and cooling processes and past history. The equilibrium of the thermal phases in the case of thermal and ionization balance and in the case of constant pressure of the plasma have been widely discussed (for references see, e.g., Lepp et al. 1985; McKee & Begelman 1990). More recent investigations are concentrated on the process of two-phases medium formation (Aranson, Meerson & Sasorov 1993) and dynamics of this medium (Elphick, Regev & Shaviv, 1992; Aharonson, Regev & Shaviv 1994).

We focus our attention on the dynamics of the thermal phases generation and separation of mass over temperatures due to the thermal instability process. We are interested in the evolution of the most rapidly growing modes which have time scales (and corresponding spacial scales) comparable with the characteristic cooling time  $t_c$ . The growth of small amplitude perturbations of temperature and of density of the optically thin medium under the action of exter-

nal heating and radiative cooling was studied by Weymann (1960) and Field (1965) in the linear approximation. The nonlinear regime is traditionally investigated by solving the exact or reduced hydrodynamical equations for the density, velocity and temperature perturbations of gas in space (see, e.g., Aranson et al. 1993). But, the detailed evolution models in these approaches can be only constructed by assuming the one-dimensional (1D) distributions. The attempts to solve this problem in two- and three-dimensions meet significant technical difficulties.

In the present paper we propose a new statistical approach to describe the dynamics of the thermal instability and construct the theory for any (linear or nonlinear) stages in isobaric approximation. In the frame of this approach we investigate the time evolution of the mass distribution function over temperature  $\varphi(T)$  [see equation (3.3)], which characterizes the statistical properties of the multiphase medium. Such a medium may contain arbitrarily spaced three-dimensional perturbations of short scales. We assume the constant gas pressure ( $P = \text{const}$ ) over volume even large contrasts of density  $\rho$  and temperature  $T$  exist. But, at the same time, the pressure is a *time dependent*

\*E-mail: illarion@dpc.asc.rssi.ru (AFI); ivi@fy.chalmers.se (IVI)

value. So, at any moment  $t$  the density and temperature of matter meet the relation  $\rho \propto P/T$ .

We show in Section 3 that in the case of the isobaric and nonuniform medium the temperature growth rate  $\dot{T}$  of the matter with temperature  $T$  [see equation (3.12)] is

$$\dot{T} \propto - \left[ \frac{1}{\gamma} \mathcal{L} + (1 - \frac{1}{\gamma}) \bar{\mathcal{L}} \frac{T}{\bar{T}} \right]. \quad (1.1)$$

Here  $\mathcal{L} = \mathcal{L}(\rho, T) = \mathcal{L}(P/T, T)$  is the local cooling-heating rate of the gas,  $\bar{\mathcal{L}}$  and  $\bar{T}$  are the mass average values of  $\mathcal{L}$  and  $T$ , respectively [see equation (3.11)], and  $\gamma$  is the gas adiabatic index. In the case of the uniform medium the equation (1.1) reduces to the form  $\dot{T} \propto -\mathcal{L}$ . One can see that the growth rate (1.1) depends on the local  $T$  only. Other quantities are common for any parts of the medium. They are the average over mass parameters, but are not independent variables. In this case  $\dot{T} = \dot{T}(T)$  the time evolution equation of the function  $\varphi(T)$  [see equation (3.15)] is of the Liouville type:

$$\frac{\partial \varphi}{\partial t} + \frac{\partial}{\partial T}(\dot{T} \varphi) = 0. \quad (1.2)$$

These coupled equations (1.1) and (1.2) determine the evolution of the medium on any (linear or nonlinear) stages.

We illustrate our statistical approach in the case of a slowly expanding interstellar cloud when the medium smoothly evolves from the thermally stable stage to the unstable stage. This evolution occurs through the critical point of marginal stability. We keep in mind the evolution of the initially ‘warm’ ( $T \simeq 10^4 \text{ K}$ ) gas because it can be in a stable equilibrium in a very wide range of the external heating and ionization parameters. The initial stages of the thermal instability follow the linear theory of Weymann (1960) and Field (1965). On the subsequent nonlinear stages, when the linear theory is not applicable, we compare the numerical solutions of the equations (1.1) and (1.2), and 1D hydrodynamical solutions. The results of both statistical and hydrodynamical approaches are identical in the isobaric limit, when the pressure is almost constant over the medium. We also estimate the limits of applicability of the statistical approach.

The hydrodynamical approach is discussed in Section 2. In Section 3 the statistical theory of thermal instability is constructed in the isobaric approximation. The smooth scenario of the thermal instability process is considered in Section 4. In Section 5 we discuss the numerical solutions of the equations of the statistical approach and hydrodynamical equations, and compare the results of both approaches. In Section 6 we discuss the obtained results and the limits of the constructed theory. In Appendix A we describe the numerical procedure of solution of the statistical equations. In Appendix B we present the results of the linear theory in the considered case of the smooth scenario.

## 2 HYDRODYNAMICAL APPROACH

The dynamics of a thermally unstable plasma can be described by the hydrodynamical equations for ideal gas with the additional cooling-heating term in the energy equation.

$$\frac{d\rho}{dt} + \rho \nabla \vec{v} = 0, \quad (2.1)$$

$$\rho \frac{d\vec{v}}{dt} + \nabla P = 0, \quad (2.2)$$

$$\frac{1}{\gamma - 1} \frac{dP}{dt} + \frac{\gamma}{\gamma - 1} P \nabla \vec{v} + \rho \mathcal{L}(\rho, T) = 0, \quad (2.3)$$

$$P = \frac{R}{\mu} \rho T. \quad (2.4)$$

Here  $\rho$ ,  $P$ ,  $T$ ,  $\vec{v}$  are the density, the pressure, the temperature, and the velocity of gas, respectively,  $R$  is the gas constant,  $\mu$  is the mean molecular weight, and  $\gamma$  is the adiabatic index. For simplicity, we do not take into account the influence of the ionization processes on thermal balance, and assume  $\gamma$  and  $\mu$  to be constant. We assume fully ionized hydrogen plasma, setting  $\gamma = 5/3$  and  $\mu = 1/2$  for numerical estimations. The cooling-heating rate  $\mathcal{L}$  is defined as the rate of energy losses minus the heating rate per unit mass. We assume that  $\mathcal{L}$  depends on the local density  $\rho$  and temperature  $T$  of gas. In the simplest case of low density and optically thin plasma (Spitzer 1962) this rate is

$$\mathcal{L}(\rho, T) = \rho \Lambda(T) - H, \quad (2.5)$$

where  $\Lambda(T)$  and  $H$  are cooling and heating rates, respectively. The heating rate of the plasma can be determined by different mechanisms (e.g., photoabsorption, Compton-effect, heating due to cosmic rays and nuclear decays). For generality, we do not specify here these mechanisms and use a constant value for the heating rate in our models. In the simplest case of a stationary medium of temperature  $T_0$  and density  $\rho_0$  the criterion of marginal stability takes the form (Weymann 1960, Field 1965)

$$\left. \frac{d}{dT} \left( \frac{\Lambda}{T} \right) \right|_{T_0} = 0, \quad \rho_0 = \frac{H}{\Lambda(T_0)}. \quad (2.6)$$

In the stable region the derivative is positive, in the unstable region it is negative. The cooling function  $\Lambda(T)$  was calculated in a number of papers (e.g., Cox & Tucker 1969; Raymond, Cox & Smith 1976) for the different conditions in the interstellar plasma. For typical conditions of thermal interstellar plasma the marginal temperature  $T_0$  is about  $10^4 \text{ K}$ . The function  $\Lambda(T)/T$  has a maximum at  $T = T_0$ . At  $T < T_0$  the plasma is thermally stable, and at  $T > T_0$  the plasma is unstable. In the presence of external ionizing (UV) radiation the function  $\Lambda(T)$  changes significantly (e.g., Krolik, McKee & Tarter 1981).

In equation (2.3) we omit the thermal conductivity term  $\nabla(\kappa \nabla T)$ , where  $\kappa$  is the thermal conductivity coefficient. The thermal conductivity process stabilizes the thermal instability at the shortest wavelengths  $\lambda \lesssim 2\pi(\kappa\mu/nR\rho)^{1/2}$ , where  $n$  is the growth rate of instability (see the discussion in Section 6). The modes of larger wavelength can be developed till the nonlinear stages. For these modes the thermal conductivity process is important at the nonlinear stage, when the medium becomes very nonuniform and is divided into cold and hot phases. The thermal conductivity effectively stabilizes the further temperature growth of the hot phase and can produce the evaporation of the cold phase. In a subsequent paper, we will analyze the influence of thermal conductivity at the nonlinear stage of the thermal instability process.

### 3 STATISTICAL APPROACH

We consider the cloud of plasma of mass  $M$  and of volume  $V$ . The equations (2.1)-(2.4) give us a precise description of the thermal and dynamical evolution of this matter. However, the solution of the problem in general case meets significant technical difficulties. We simplify the analysis proposing a new statistical approach which is constructed under isobaric approximation. The isobaric condition corresponds to a short wavelength limit

$$\lambda \lesssim \lambda_P = 2\pi c_s t_c, \quad (3.1)$$

when the pressure balance time  $\sim \lambda/c_s$  is shorter than the characteristic thermal time

$$t_c = \frac{c_s^2}{H}. \quad (3.2)$$

Here  $c_s = (\gamma P/\rho)^{1/2}$  is the adiabatic sonic speed. The hydrodynamical calculations confirm (see Section 5) that in the wavelength range (3.1) the isobaric approximation is satisfied. The calculations also set the limits of applicability of the statistical approach.

We build our theory using the temperature-dependent distribution of matter instead of the space-dependent one. We sum the masses of equal temperature and compose the distribution function  $\varphi(T)$  of mass over temperature. Namely, the mass of gas  $\Delta m$  having the temperature in the range from  $T$  to  $T + \Delta T$  is

$$\Delta m = M\varphi(T)\Delta T, \quad (3.3)$$

where the distribution function  $\varphi(T)$  is normalized to unity

$$\int_0^\infty \varphi(T)dT = 1. \quad (3.4)$$

Now we show that the temperature growth rate  $\dot{T}$  depends only on local  $T$  and the global (average) parameters of the medium. First we prove that for isobaric perturbations the pressure of the gas

$$P = \frac{R}{\mu} \frac{M}{V} \bar{T} \quad (3.5)$$

is determined by the mass average temperature

$$\bar{T} = \int_0^\infty T\varphi(T)dT, \quad (3.6)$$

and the average density of the cloud  $\langle \rho \rangle = M/V$ . Indeed, using equations (2.4) and (3.3) we can write

$$V = \int_M \frac{dm}{\rho} = \int_0^\infty \frac{M\varphi(T)dT}{\rho} = \frac{R}{\mu} M \int_0^\infty \frac{T\varphi(T)dT}{P}. \quad (3.7)$$

In the isobaric case  $P = \text{const}$  the equation (3.5) follows from (3.7) directly.

Second, from equations (2.1) and (2.4) we have for the velocity divergency

$$\nabla \vec{v} = -\frac{\dot{\rho}}{\rho} = -\frac{\dot{P}}{P} + \frac{\dot{T}}{T}. \quad (3.8)$$

Substituting  $\nabla \vec{v}$  into equation (2.3) we obtain the relation between temperature and pressure growth rates

$$\dot{T} = \frac{\gamma-1}{\gamma} \left( \frac{\dot{P}}{P} T - \frac{\mu}{R} \mathcal{L} \right). \quad (3.9)$$

Third, taking the average in (3.9) we set  $\bar{T} = PV\mu/MR$  [see equation (3.5)] instead of  $T$  in the right side and correspondingly  $(\dot{P}V)\mu/MR$  instead of  $\dot{T}$  in the left side, and find for the pressure derivative

$$\dot{P} = -(\gamma-1) \frac{M}{V} \bar{\mathcal{L}} - \gamma \frac{\dot{V}}{V} P. \quad (3.10)$$

Here and below the mass average of any function  $A(T)$  is defined as

$$\bar{A} = \int_0^\infty \varphi(T)A(T)dT. \quad (3.11)$$

Finally, substituting  $\dot{P}$  from (3.10) into (3.9) we have the temperature growth rate of the matter with temperature  $T$ :

$$\dot{T} = -\frac{\gamma-1}{\gamma} \frac{\mu}{R} \left[ (\gamma-1) \bar{\mathcal{L}} \frac{T}{\bar{T}} + \mathcal{L} \right] - (\gamma-1) \frac{\dot{V}}{V} T. \quad (3.12)$$

This equation follows from the mass (2.1) and energy (2.3) conservation equations. Instead of the Euler equation (2.2) we use the isobaric condition  $P = C = \text{const}$ . Hydrodynamical calculations give us that  $P = C + O(\lambda^2)$  (see Appendix B), but we ignore here the additional term  $O(\lambda^2)$  in the  $\lambda \lesssim \lambda_P$  limit.

Note, that small velocities on small scales provide a scale-independent value of the velocity divergency,  $\nabla \vec{v} \sim v_\lambda/\lambda$ . One can substitute (3.10) and (3.12) into (3.8) and obtain explicitly

$$\nabla \vec{v} = \frac{\gamma-1}{\gamma} \frac{\mu}{R} \left( \frac{\bar{\mathcal{L}}}{\bar{T}} - \frac{\mathcal{L}}{T} \right) + \frac{\dot{V}}{V}, \quad (3.13)$$

which is determined only by the local temperature  $T$ .

In the isobaric case, according to (2.4) and (3.5) we have for density  $\rho = \langle \rho \rangle \bar{T}/T$ . It has to be set in the function  $\mathcal{L}(\rho, T)$  everywhere. For example, the rate  $\mathcal{L}$ , determined by formula (2.5), and its average value  $\bar{\mathcal{L}}$ , both of which we need to put into equations (3.12) and (3.13), have forms

$$\mathcal{L} = \langle \rho \rangle \frac{\Lambda(T)}{T} \bar{T} - H, \quad \bar{\mathcal{L}} = \langle \rho \rangle \left( \frac{\bar{\Lambda}}{\bar{T}} \right) \bar{T} - H. \quad (3.14)$$

After that we have all of the parameters  $(\mathcal{L}, \bar{\mathcal{L}}, \bar{T})$  to substitute to formula (3.12) for the rate  $\dot{T}$ . Also we have formulae for the pressure (3.5) and the velocity divergency (3.13) of the medium.

The time evolution of the mass distribution  $\varphi(T)$  we describe by the Liouville type equation

$$\frac{\partial \varphi}{\partial t} + \frac{\partial}{\partial T} (\dot{T} \varphi) = 0, \quad (3.15)$$

where the temperature growth rate  $\dot{T}$  is given by formula (3.12). The equation (3.15) is nonlinear because the term  $\dot{T}$  depends on the function  $\varphi(T)$  through the average values  $\bar{T}$  and  $\bar{\mathcal{L}}$ . If we specify the initial conditions at the moment  $t_i$ , the cooling-heating function  $\mathcal{L}(\rho, T)$  and the law of expansion of the medium  $V(t)$ , then the equations (3.12) and (3.15) describe the thermal evolution of medium for  $t > t_i$ . The initial conditions are the distribution function  $\varphi(T, t_i)$  and mean density  $\langle \rho \rangle_i$ . To solve the equations (3.12) and (3.15) we use a numerical technique (see Appendix A) in the general case of finite amplitude perturbations.

The evolution equation for the relative temperature perturbation  $\delta T/\bar{T}$ , where  $\delta T = T - \bar{T}$ , can be constructed using

equation (3.12) for  $\dot{T}$  and its average version for  $\dot{\bar{T}}$ . One can get

$$\frac{d}{dt} \left( \frac{\delta T}{\bar{T}} \right) = \frac{\gamma-1}{\gamma} \frac{\mu}{R\bar{T}} \left( \bar{\mathcal{L}} \frac{T}{\bar{T}} - \mathcal{L} \right).$$

Under linear approximation we can write  $\mathcal{L}(T) = \mathcal{L}(\bar{T}) + (\partial \mathcal{L} / \partial T)_P \delta T$  and find  $\bar{\mathcal{L}} = \mathcal{L}(\bar{T})$ , because of  $\delta \bar{T} = 0$ . In this case the equation for the relative temperature perturbation becomes

$$\frac{d}{dt} \left( \frac{\delta T}{\bar{T}} \right) = \frac{\gamma-1}{\gamma} \frac{\mu}{R\bar{T}} \left( \mathcal{L} - \left( \frac{\partial \mathcal{L}}{\partial T} \right)_P \bar{T} \right) \frac{\delta T}{\bar{T}}. \quad (3.16)$$

Here the values of  $\mathcal{L}$  and  $(\partial \mathcal{L} / \partial T)_P$  are taken at  $T = \bar{T}$ . For example, in case of the static uniform medium at the thermal equilibrium  $\mathcal{L}(\bar{T}) = 0$  we find the growth rate

$$n = \frac{\gamma-1}{\gamma} \frac{\mu}{R\bar{T}} \left( \langle \rho \rangle \left( \frac{\partial \mathcal{L}}{\partial \rho} \right)_T - \bar{T} \left( \frac{\partial \mathcal{L}}{\partial T} \right)_\rho \right), \quad (3.17)$$

which coincides with the growth rate found by Weymann (1960) and Field (1965). For the cooling-heating function (2.5) it is reduced to

$$n = \frac{\gamma-1}{t_c} \left( 1 - \frac{T}{\Lambda} \frac{d\Lambda}{dT} \right), \quad (3.17')$$

where  $t_c$  is given by (3.2). From equation (3.17') one can obtain the criterion (2.6).

Finally we note the following:

1. One can construct uniquely the distribution function  $\varphi(T)$  from any  $T(\vec{r})$  summing the correspondent masses of volumes  $\Delta V_i$  with temperatures in range from  $T$  to  $T + \Delta T$ ,

$$\varphi(T) \Delta T = \frac{\rho \sum_i \Delta V_i}{M}.$$

For instance, consider a one dimensional case and the cosine profile of temperature,  $T(x) = T_0 - \delta T_0 \cos(2\pi x/\lambda)$ . Then we can obtain inverse dependence  $x(T)$  for the interval  $0 < x < \lambda/2$  of monotonicity of  $T(x)$  and find the distribution function

$$\varphi(T) = \frac{2 \bar{T}}{\lambda T} \frac{dx(T)}{dT} = \frac{1}{\pi T} \frac{1}{\sqrt{\delta T_0^2 - (T - T_0)^2}}, \quad (3.18)$$

$T_0 - \delta T_0 < T < T_0 + \delta T_0,$

where the mass average  $\bar{T} = \sqrt{T_0^2 - \delta T_0^2}$ , and  $\delta T_0 < T_0$ . The dispersion  $\sigma_T^2 = (T - \bar{T})^2 / \bar{T}^2 \approx \frac{1}{2} (\delta T_0 / T_0)^2$  at  $\delta T_0 \ll T_0$ . The function (3.18) is independent of the space period  $\lambda$  and has two integrable infinities at  $T_{min} = T_0 - \delta T_0$  and  $T_{max} = T_0 + \delta T_0$  as shown in Fig. 1.

2. The reconstruction of the space distribution  $T(\vec{r})$ ,  $\rho(\vec{r})$  and velocity field  $\vec{v}(\vec{r})$  from a given  $\varphi(T)$  is an incorrect procedure. The recovery can be uniquely done in the one dimensional case assuming additional restrictions on the temperature profile  $T(x)$ . The temperature must be a periodical, monotonical for one half period ( $0 < x < \lambda/2$ ) and odd symmetrical (relative  $x = 0$ ) function. Keeping this restrictions one can find the implicit dependence  $T(x)$ :

$$2 \frac{x}{\lambda} = \frac{1}{\bar{T}} \int_0^{T(x)} T' \varphi(T') dT'. \quad (3.19)$$

Then for the density distribution we have

$$\rho(x) = \langle \rho \rangle \bar{T} / T(x). \quad (3.20)$$

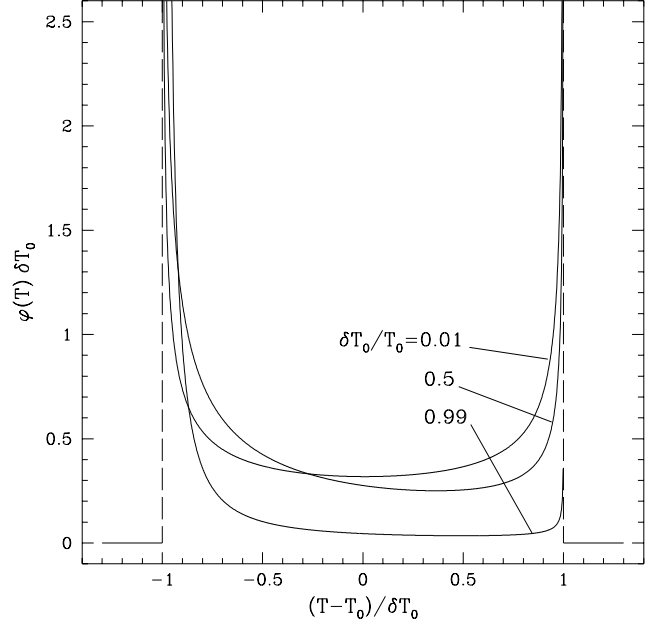


**Figure 1.** The distribution function  $\varphi(T)$  in the case of the cosine profile  $T(x) = T_0 + \delta T_0 \cos(2\pi x/\lambda)$  for different values of relative amplitude  $\delta T_0/T_0 = 0.01, 0.5, 0.99$ .

The velocity profile can be obtained by integrating equation (3.13):

$$v(x) = \tilde{v}(x) + \frac{\dot{V}}{V} x =$$

$$\frac{\gamma-1}{\gamma} \frac{\mu}{R\bar{T}} \frac{\lambda}{2} \int_0^{T(x)} \left( \bar{\mathcal{L}} \frac{T'}{\bar{T}} - \mathcal{L}(T') \right) \varphi(T') dT' + \frac{\dot{V}}{V} x. \quad (3.21)$$

The amplitude of the perturbed part  $\tilde{v}(x)$  of  $v(x)$  is proportional to the space period  $\lambda$ , and  $\tilde{v}(0) = \tilde{v}(\lambda/2) = 0$ .

## 4 SMOOTH SCENARIO

We illustrate our statistical theory of thermal instability in the case of inertially expanding uniform plasma cloud. The density of the cloud decreases with time, say,

$$\rho_u(t) \propto \frac{1}{t^3}. \quad (4.1)$$

Initially the plasma is assumed to be quite dense and cold. The temperature  $T_u$  of the uniform plasma is less than the marginal value  $T_0$ , and the plasma is thermally and mechanically stable [see condition (2.6) and subsequent discussion]. In the case of a constant heating rate  $H$  the temperature  $T_u$  increases up to the marginal temperature  $T_0$ . It happens at some moment  $t_0$ . At time  $t > t_0$  the plasma is unstable.

Numerical models show (see Section 5.1) that the fragmentation of cloud is only possible in the case of a ‘slowly’ expanding cloud for which the characteristic thermal time  $t_c$  [equation (3.2)] is much shorter than expanding time  $t_0$ . In this case  $t_c \ll t_0$  the thermal (quasi) equilibrium of uniform matter is established,  $\mathcal{L} = 0$ . Then the evolution of temperature  $T_u(t)$  follows from the equation

$$\Lambda(T_u) = \frac{H}{\rho_u} = \Lambda(T_0) \left( \frac{t}{t_0} \right)^3. \quad (4.2)$$

Near the marginal point  $T_0$  (where  $\Lambda = Td\Lambda/dT$ ) one can find

$$T_u(t) = T_0(1 + 3\frac{\delta t}{t_0}), \quad (4.2')$$

where  $\delta t = t - t_0 \ll t_0$ .

In the thermally unstable plasma the fastest growth rate has a condensation mode which corresponds to the conditions  $\lambda \lesssim \lambda_P$  and  $P \approx \text{const}$ . In the linear regime the amplitude  $A$  of this mode follows the equation  $\dot{A} = nA$ . At  $\delta t \ll t_0$  the growth rate  $n$  is small and linearly proportional to  $\delta t$ :

$$n(t) = 3b\frac{\gamma - 1}{t_c}\frac{\delta t}{t_0}, \quad (4.3)$$

where  $b = -T_0^2\Lambda''(T_0)/\Lambda(T_0)$  is the positive quantity. The formula (4.3) follows from equation (3.17'), where the term in the brackets can be linearly approximated  $1 - T\Lambda'/\Lambda = -T_0(T - T_0)\Lambda''/\Lambda$  at the limit  $T - T_0 \ll T_0$ . In addition the time dependency of temperature (4.2') is used. Here and below we define the parameter  $t_c = c_s^2(T_0)/H$  at the moment  $t = t_0$ . On the linear stage (Weymann 1960, Field 1965, see also Appendix B) at  $0 < \delta t < \tau$ , the amplitude increases as

$$A(t) = A_0 \exp N(t), \quad N(t) = \int_{t_0}^t n dt = \frac{3}{2}b\frac{\gamma - 1}{t_c}\frac{\delta t^2}{t_0}, \quad (4.4)$$

and we must study the progressively inhomogeneous medium. Equation (4.1) is then correct for the average density  $\langle \rho \rangle$  only. The linear regime is limited by the time interval  $0 < \delta t < \tau$ , where the end time

$$\tau = \sqrt{\frac{2t_0t_c \ln(1/A_0)}{3b(\gamma - 1)}}. \quad (4.5)$$

At  $\delta t = \tau$  the integral  $N = \ln(1/A_0)$  and the amplitude  $A = 1$ . At  $t > t_0 + \tau$  the perturbations are large and grow nonlinearly. In case of the small parameter  $t_c/t_0 \ll 1$ , the time interval of the linear stage is also small:  $\tau/t_0 \approx \sqrt{\ln(1/A_0)t_c/t_0} \ll 1$ .

The scenario of the expanding cloud is able to follow the natural smooth evolution of the medium from the stable ( $t < t_0$ ,  $T < T_0$ ) to the unstable ( $t > t_0$ ,  $T > T_0$ ) stages through the critical point ( $T = T_0$ ). Other scenarii of a smooth transition through the critical point  $T = T_0$  can also be constructed. For example, we can take the stationary medium ( $\rho_u = \rho_0 = \text{const}$ ) heated at a slowly increasing rate and obtain similar results assuming  $t_c \ll t_0$  and setting  $H(t) = H_0(t/t_0)^3$ ,  $H_0 = \rho_0\Lambda(T_0)$ .

## 5 NUMERICAL RESULTS

We use the expanding cloud scenario to numerically study the thermal instability process in the framework of statistical isobaric theory. We find numerically the time evolution of the distribution function  $\varphi(T, t)$  and the evolution of corresponding characteristic parameters of this distribution. We also find the final mass fraction of cold and hot phases as a function of the parameters of the problem. To test the results of the statistical approach we compare them with the results of hydrodynamical calculations in the following way. We use the obtained  $\varphi(T, t)$  to construct the  $T(x)$ ,  $\rho(x)$  and  $v(x)$  profiles. To do this we use the reconstruction procedure,

which is discussed at the end of Section 3 [see equations (3.19), (3.20) and (3.21)]. After this we compare the constructed profiles with the profiles resulting from the 1D hydrodynamical calculations under the identical parameters of the problem and the similar initial conditions. In all models we fix the heating rate  $H = \text{const}$  and set  $\gamma = 5/3$ ,  $\mu = 1/2$ . The expansion law (4.1) for the average density  $\langle \rho \rangle$  of the plasma is assumed in the calculations.

We use the model curve of the cooling function  $\Lambda(T)$ , which mimics the base properties of the cooling processes in the interstellar plasma,

$$\Lambda(T) = \Lambda_0 \frac{2(T/T_0)^2}{1 + (T/T_0)^2} \theta(T), \quad (5.1)$$

where the function  $\theta(T)$  is

$$\theta(T) = \begin{cases} 1, & \text{if } T/T_0 > c, \\ \exp[d(1/c - T_0/T)], & \text{otherwise.} \end{cases}$$

Here we assume  $c = 0.9$  and  $d = 10.0$ . The exponential drop of  $\theta(T)$  in the low temperature region  $T < cT_0$  mimics the strong fall of  $\Lambda(T)$ . The cooling curve (5.1) has the critical point  $T = T_0 = 10^4 K$ , where the criterion of marginal stability (2.6) is fulfilled. The instability growth rate coefficient [see equation (4.3)]  $b = 1$  in this case. We note, that the cooling curve (5.1) does not allow a stable equilibrium for a two-phases medium.

We start our calculations at moment  $t = t_0$ . The initial relative perturbations of temperature  $\Delta = (T_{\max} - T_{\min})/\bar{T}$  and the expansion parameter  $t_0/t_c = t_0 H/c_s^2(T_0)$  are free parameters of the models. The hydrodynamical models, in addition, are characterized by the initial space period  $\lambda_0/\lambda_P$  of perturbations. Here  $\lambda_P = 2\pi c_s^3(T_0)/H = 2\pi c_s t_c$ .

The cosine profile of temperature  $T(x) = T_0(1 - \frac{\Delta}{2} \cos(2\pi x/\lambda_0))$  is used as the initial perturbations in the hydrodynamical models. In the statistical models the corresponding initial distribution function  $\varphi(T)$  is given by equation (3.18). The initial temperature dispersion  $\sigma_T^2(t_0) = \Delta^2/8 = A_0^2/2$ .

### 5.1 Statistical isobaric models

The numerical method used to solve the equations (3.12) and (3.15) of statistical approach is briefly described in Appendix A.

We discuss, as a characteristic example, the detailed evolution of the S-model, with the initial parameters  $\Delta = 10^{-4}$  and  $t_0/t_c = 10^4$ . The temperature dispersion  $\sigma_T^2 = (T - \bar{T})^2/\bar{T}^2$  increases with time at the  $t > t_0$  stage. The evolution of  $\sigma_T(t)$  is shown in Fig. 2. Initially  $\sigma_T(t_0) = \Delta/\sqrt{8}$ . The solid line corresponds to the nonlinear calculation, and the dashed curve was calculated under the linear approximation [equation (3.16)]. As it was shown in Section 4 [equation (4.4)] at the linear stage  $\sigma_T(t) \approx \sigma_T(t_0) \exp[(t - t_0)^2/t_0 t_c]$ . A significant deviation is observed between the linear and nonlinear stages when the value of  $\sigma_T$  is large,  $\sigma_T \gtrsim 0.1$ . The instability results in the formation of the two-phases medium at the moment  $t \approx t_0 + \tau$ , where the time interval  $\tau$  is determined by equation (4.5).

In Fig. 3 (left- and right-hand panels) we show the trajectories of mass particles in  $(T, t)$ -plane. Each line is the

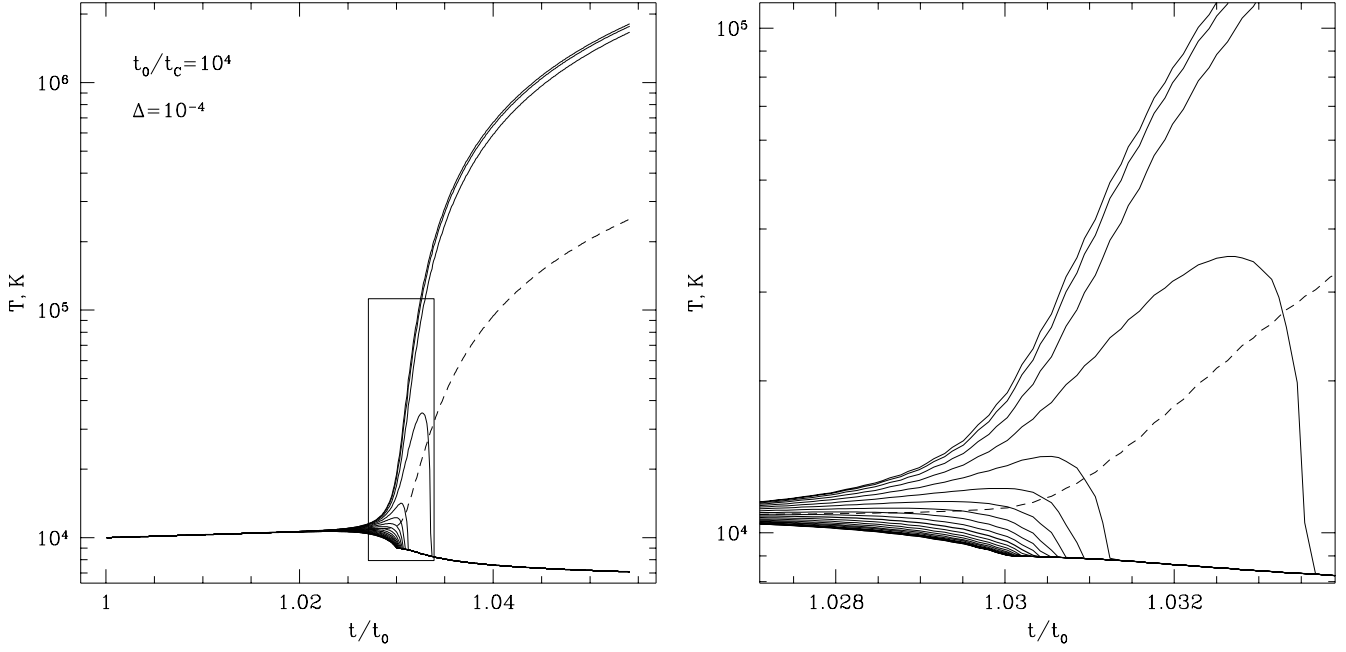


**Figure 3.** The evolution of temperatures of the fixed mass coordinates (solid lines) and average temperature  $\bar{T}$  (dashed line) for the S-model. The mass coordinates of neighbouring solid lines differ by  $\Delta M/M = 0.05$ . The upper and lower lines correspond to maximum and minimum temperature of plasma. The long time evolution is shown in the left-hand panel. Detailed evolution at right represents the nonlinear stage shown inside the box in the left-hand panel.

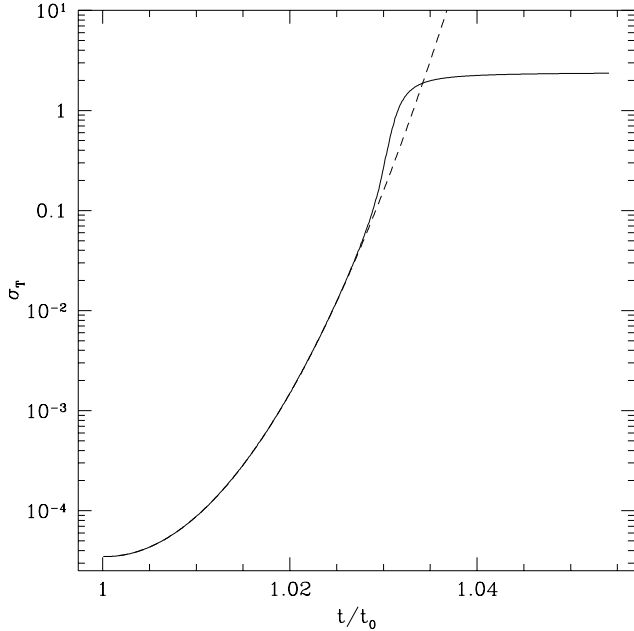


**Figure 2.** The evolution of the relative perturbation of temperature  $\sigma_T$  for the statistical isobaric S-model. The solid line shows the evolution coming from nonlinear theory, and the dashed line shows the result in the linear approximation.

trajectory of a fixed mass coordinate, and for each two neighbour lines  $\ell_1$  and  $\ell_2$  the following condition is satisfied:

$$\frac{\Delta M}{M} = \int_{T(\ell_1)}^{T(\ell_2)} \varphi(T') dT' = 0.05,$$

for any time  $t$ . The upper and lower lines correspond to max-

imum and minimum temperatures of plasma. The dashed line shows the evolution of average temperature  $\bar{T}(t)$ . Note, that the time dependence of  $\bar{T}(t)$  does not coincide with the evolution of temperature of the uniform medium followed from equation (4.2). In the linear stage of instability the lines are spaced closely. In the nonlinear stage, which is approximately shown inside the box in the left-hand panel and in more detail in the right-hand panel of Fig. 3, the lines disperse rapidly. One group of lines goes up to the high temperatures, and another group goes down to the low temperatures. A small part of gas of intermediate temperatures shows nonmonotonic behaviour in its temperature evolution.

At the following time  $t > t_0 + \tau$  the two-phase medium with hot ( $T_h, \rho_h$ ) and cold ( $T_c, \rho_c$ ) phases is formed. A sharp boundary separates phases. Numerical calculations show that the mass fraction of the cold and hot phases tend asymptotically to final values. In the case of the S-model the final fraction of the cold mass is  $\eta = 0.86$ . The remainder  $1 - \eta = 0.14$  is the final mass fraction of the hot matter. The temperature dispersion of this medium is

$$\sigma_T^2 = \left( \frac{T_h}{\bar{T}} - 1 \right)^2 (1 - \eta) + \left( 1 - \frac{T_c}{\bar{T}} \right)^2 \eta.$$

In the limit  $T_c \ll T_h$  one obtains a simple relation  $\sigma_T^2 = \eta/(1 - \eta)$ . For the case  $\eta = 0.86$ , we find  $\sigma_T = 2.5$ , which very well agrees with our numerical result (see Fig. 2).

Consider now the evolution of the parameters of hot and cold phases at the stage  $t - t_0 \ll t_0$ , when the expansion can be neglected. Assuming  $T_h \gg T_c$  one can substitute in equation (2.3) the density of hot gas  $\rho_h = \langle \rho \rangle_0 (1 - \eta)$ , where  $\langle \rho \rangle_0 = H/\Lambda_0$ , and obtain the equation:

$$\dot{T}_h = (\gamma - 1) \frac{\mu}{R} H \left( \frac{\Lambda(T_h)}{\Lambda_0} (\eta - 1) + 1 \right). \quad (5.2)$$

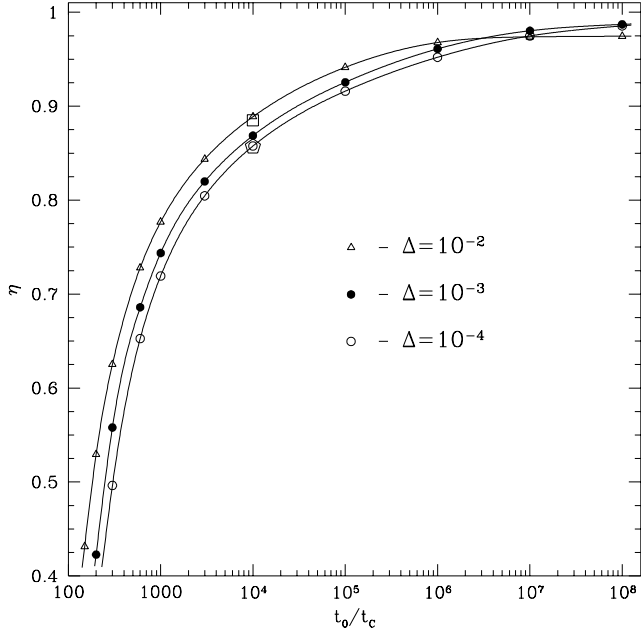


**Figure 4.** The final mass fraction of cold phase  $\eta$  of the statistical isobaric models as a function of the expansion parameter  $t_0/t_c$  for the initial amplitudes  $\Delta = 10^{-2}$ ,  $10^{-3}$  and  $10^{-4}$  (deltas, full circles and open circles). A pentagon and square show the final mass fractions of the hydrodynamical H1 and H2-models, respectively, which have the initial amplitude  $\Delta = 10^{-4}$ . The H1-model and isobaric S-model (at  $t_0/t_c = 10^4$  and  $\Delta = 10^{-4}$ ) have almost equal final mass fractions.

The ratio  $\Lambda(T_h)/\Lambda_0 = 2$  [see formula (5.1)] and we obtain  $\dot{T}_h \sim (2\eta - 1)$ . The temperature of the hot phase increases to infinity and a two-phase medium can be formed in the case when more than half of the matter falls down to the cold phase,  $\eta > 1/2$ . Finally, at  $t > t_0 + \tau$ , we have

$$T_h \simeq (\gamma - 1) \frac{\mu}{R} H(2\eta - 1)(t - t_0 - \tau).$$

The numerical calculations confirm this estimation. The temperature  $T_c$  and density  $\rho_c$  of cold phase are determined by the condition of thermal equilibrium  $H = \rho_c \Lambda(T_c)$  and the isobaric relation with hot phase, which corresponds to the relation  $\rho_c = \langle \rho \rangle_0 [(1 - \eta)T_h/T_c + \eta]$ .

The final mass fraction of the phases is an important characteristic of the models. We studied the dependence of the mass fraction  $\eta$  on the parameters  $\Delta$  and  $t_0/t_c$ . Fig. 4 shows  $\eta$  as a function of  $t_0/t_c$  for three values of the initial amplitude  $\Delta = 10^{-2}$ ,  $10^{-3}$ ,  $10^{-4}$ . In the case of a slowly expanding limit  $t_0/t_c \gtrsim 10^4$  the mass fraction  $\eta$  is a slowly increasing function of  $t_0/t_c$  and weakly ( $< 5\%$ ) depends on  $\Delta$ , when  $\eta \gtrsim 0.85$ . In case of a fast expansion  $t_0/t_c \lesssim 10^3$ , the mass fraction  $\eta$  decreases, and its dependence on  $\Delta$  becomes significant. The value of  $\eta$  reaches the minimum  $\approx 0.4$  at  $t_0/t_c \approx 10^2$ , when the end time of the linear stage  $\tau \approx 0.3t_0$  [see equation (4.5)] becomes equal to the expansion time  $V/\dot{V} \simeq t_0/3$  [see equation (4.1)]. For a faster expanding medium,  $t_0/t_c \lesssim 10^2$ , the final two-phase structure is not developed. In this case the expansion factor suppresses the thermal instability, and the models show the initial growth of the dispersion  $\sigma_T^2$  until some maximum and the following decrease. The medium remains hot and uniform.

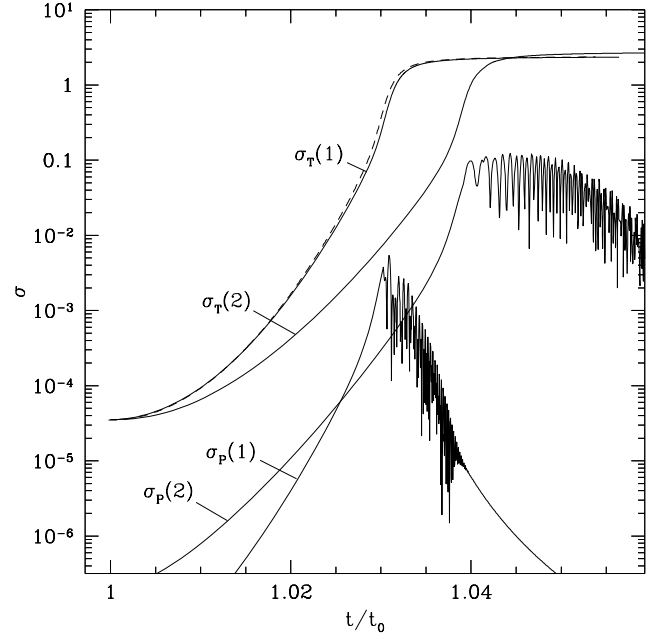


**Figure 5.** The evolution of relative perturbations of temperature  $\sigma_T$  and pressure  $\sigma_P$  for H1-model and H2-model [solid lines, labeled as (1) and (2), respectively]. The evolution of temperature perturbations for the S-model (as in Fig. 2) is shown by a dashed line for comparison.

The reconstructed 1D space distributions of density and perturbed velocity for one period  $0 < x < \lambda$  are shown in Figs 6 and 7 as dashed lines. The lines are presented at subsequent moments, and the period  $\lambda$  increases with time as  $\lambda(t) = \lambda_0 t/t_0$ . The used reconstruction procedure is discussed in Section 3.

## 5.2 Hydrodynamical models

To solve equations (2.1)–(2.4) in the one-dimensional case we used an implicit hydrodynamical code. The code is based on the Lagrangian fully conservative numerical scheme of the second order accuracy (Samarskij & Popov 1980).

We discuss here two models, which differ in the initial wave length  $\lambda_0$  of perturbations,  $\lambda_0 = \lambda_P$  (H1-model) and  $\lambda_0 = 5\lambda_P$  (H2-model). They have the initial parameters  $\Delta = 10^{-4}$  and  $t_0/t_c = 10^4$ , which are identical to the S-model (see previous Section 5.1). In addition, we assume that the initial perturbed velocities and pressure variations equal to zero. The computed characteristics of the S-model almost coincide with those of the H1-model. However the H2-model shows significant differences from both S and H1 models in the linear and nonlinear stages. Fig. 5 shows the relative perturbations (square root of the correspondent dispersion) of temperature  $\sigma_T$  and pressure  $\sigma_P$  as functions of time for H1 and H2 models (solid lines). In the same Fig. 5 the evolution of  $\sigma_T$  for the S-model is shown for comparison (dashed line). The differences between the curves  $\sigma_T(t)$  for H1 and H2 models are explained by the time delay. This time delay arises in the linear stage of evolution due to differences of the growth rates of different modes (see Appendix B, Table B1). The perturbations for the shorter wave models grow more rapidly, and the most rapid growth rate is observed for

the isobaric S-model, which corresponds to the limit  $\lambda \rightarrow 0$ . The shape of  $\sigma_T$  curves for H1 and H2 models are very similar in the nonlinear stage ( $\sigma_T > 0.1$ ), but delayed in time.

To study the problem of nonlinear interaction of the modes with different  $\lambda_0$  we calculated the number of models where the initial conditions were taken as a superposition of two modes,  $\lambda_0 = \lambda_P$  and  $\lambda_0 = 5\lambda_P$ . In the case of equal initial amplitudes of the modes the long wave mode was totally suppressed by the short wave mode in the nonlinear phase. The long wave mode suppresses the development of the short wave mode when the ratio of the initial amplitudes  $\gtrsim 50$ . This result quantitatively well agrees with the estimations made in the linear theory (Appendix B). Indeed, from Table B1 one can find the difference of the exponential factors of these two modes  $\Delta N = 9.56 - 6.0 = 3.56$ . It gives us the ratio of amplitudes  $\exp(3.56) = 35$ .

The small value of relative pressure perturbation  $\sigma_P$  ( $\lesssim 10^{-2}$ ) is an indicator of the isobaricity of the process. Both H1 and H2 models have peak-like  $\sigma_P(t)$  curves (see Fig. 5), and the peaks are located at the end of the linear evolution stage, when the most rapid growth of temperature perturbations takes place. In the case of the H1-model the maximum of  $\sigma_P$  has a rather small value  $\sigma_{Pmax} \simeq 0.005$  and even at the nonlinear stage the process is almost isobarical. This value of  $\sigma_{Pmax}$  can be compared with the correspondent value followed from the linear theory,  $\sigma_{Pmax} \approx \alpha = 0.006$  (see Appendix B, Table B1). After the peak  $\sigma_P$  decreases rapidly. At this stage the sonic waves are generated during the contraction of the cold phase. These waves produce oscillations in  $\sigma_P$  clearly seen in Fig. 5. The intensity of the oscillations also rapidly decrease with time. In the case of the H2-model the relative perturbations of pressure reaches a rather high value  $\sigma_{Pmax} \simeq 0.1$  (the linear theory gives 0.067, see Table B1) and slowly decreases in oscillation regime after the maximum.

The density and velocity distributions for the H1-model are presented in Figs 6 and 7 (solid lines) at subsequent moments. In the same figures the correspondent distributions for the isobaric S-model (dashed lines) are also shown. One can see a very good coincidence between these two models. In Figs 6 and 7 the curves for the H1-model are used with the time shift  $8t_c$  with respect to the moments for the curves for the S-model. This shift follows from the time delay arising during the linear stage of evolution of both models (see Appendix B). The shift is clearly seen as a small divergence of the  $\sigma_T$  curves for the S and H1 models in Fig. 5.

The density distributions of the H2-model are shown in Fig. 8 at subsequent moments. The qualitative difference of density distributions in the H1 and H2 models consists of the origin of ‘wave hunches’ in the latter case, when the cold phase is compressed by the hot phase. The wave hunches have a time period of about  $2\pi t_c(\lambda_0/\lambda_P)$ . The origin of wave hunches indicates that the compression zone of the cold phase at the nonlinear stage is restricted by the zone of sonic wave propagation.

The final mass fractions of the cold phase  $\eta = 0.86$  and  $0.885$  for the hydrodynamical H1 and H2-model are shown in Fig. 4 by a pentagon and square, respectively. The longer wave H2-model has the larger value of  $\eta$ .

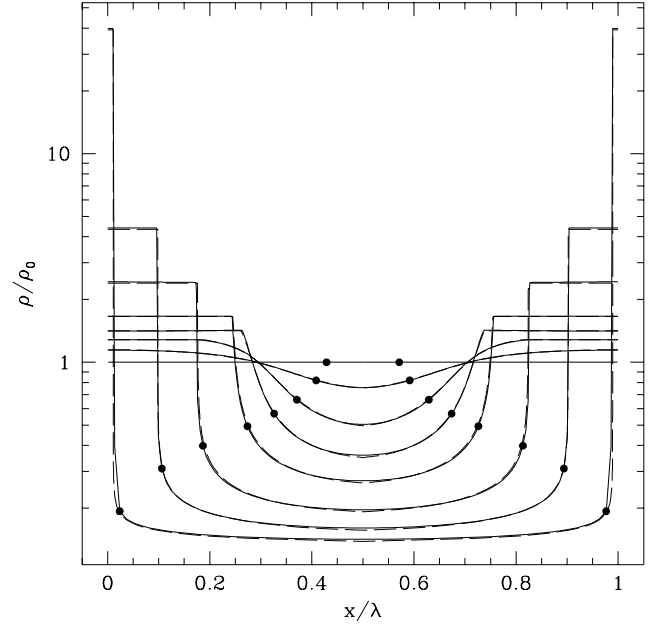


**Figure 6.** The density distributions at subsequent moments  $t/t_0 = 1.0290, 1.0300, 1.0305, 1.0311, 1.0321, 1.0339$  and  $1.0560$  for the isobaric S-model (dashed lines) and hydrodynamical H1-model (solid lines). The density distributions of these models are almost identical through the evolution. The full circles show the locations of the mass coordinate, which will finally divide cold and hot phases.

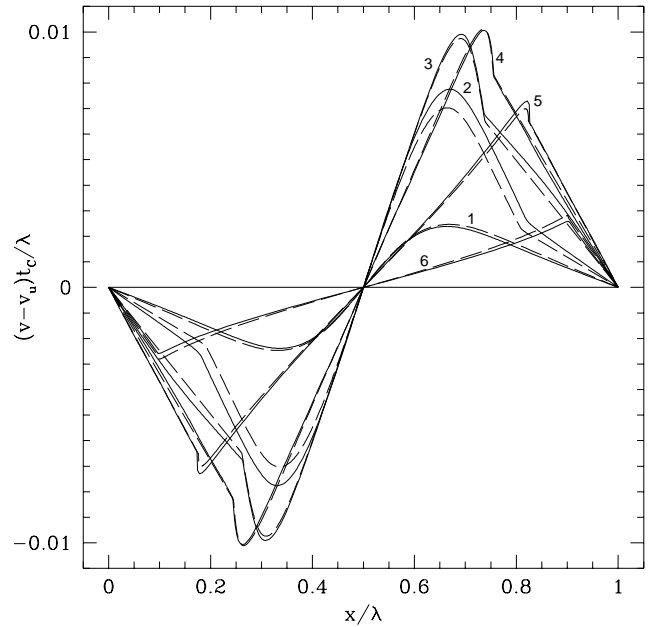


**Figure 7.** The distributions of velocity at subsequent moments (labeled by the numbers)  $t/t_0 = 1.0290, 1.0300, 1.0305, 1.0311, 1.0321$  and  $1.0339$  for the isobaric S-model (dashed lines) and hydrodynamical H1-model (solid lines).



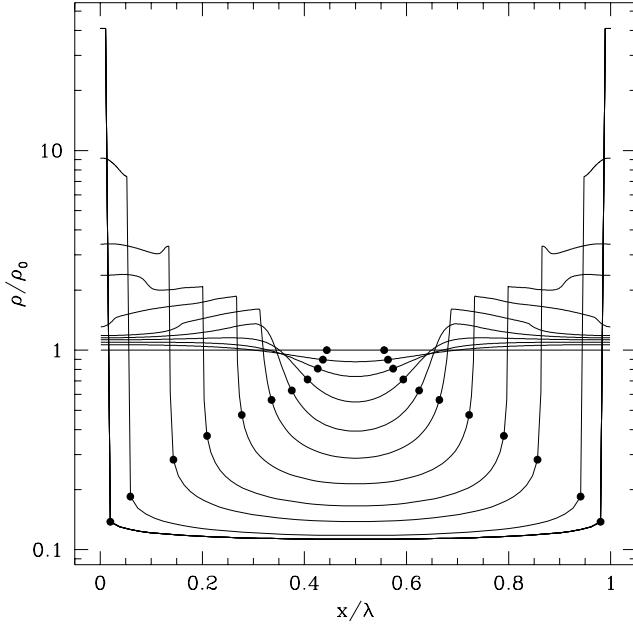


**Figure 8.** As in Fig. 6, but for hydrodynamical H2-model. The origin of ‘wave hunches’ in the cold and dense phase, which are not seen in Fig. 6 for the H1-model, indicates the breaking of the isobaric condition.

## 6 DISCUSSION AND CONCLUSION

We have developed a new statistical approach to study the thermal instability in an optically thin plasma. We investigate the time evolution of the mass distribution function over temperature  $\varphi(T)$ , which characterizes the statistical properties of the medium. This medium can contain arbitrary spaced three-dimensional perturbations. We construct the time evolution equation of function  $\varphi(T)$ , which describes perturbations of arbitrary amplitude and is correct under the isobaric condition. Formally, the obtained evolution equation does not explicitly depend on the length scale  $\lambda$  of perturbations, but the isobaric condition restricts the characteristic length of perturbations,  $\lambda \lesssim \lambda_P = 2\pi c_s t_c$ .

The reconstruction of the space distributions of the density, temperature and velocity field from the given  $\varphi(T)$  is an incorrect procedure (but we can recover these distributions under the restricted assumptions of the temperature profile). However, the statistical approach may be useful to give us the average parameters of the inhomogeneous medium, such as the pressure  $P = \frac{R}{\mu} \langle \rho \rangle \overline{T}$ , the total  $L = \int \rho^2 \Lambda(T) dV = \langle \rho \rangle M \overline{T} \left( \frac{\Lambda}{T} \right)$  and spectral  $L_\epsilon = \int \rho^2 \Lambda_\epsilon(T) dV = \langle \rho \rangle M \overline{T} \left( \frac{\Lambda_\epsilon}{T} \right)$  luminosities.

We study the evolution of function  $\varphi(T)$  numerically in the frame of the slowly expanding cloud scenario (see Section 4). We follow the thermal instability process in the linear and nonlinear stages including the formation of a two-phase medium. In the calculations we use the cooling-heating function (5.1), which does not allow the existence of a two-phases equilibrium. We find that in the case of the expanding medium the mass fractions of the phases have final nonzero values, contrary to the case of the stationary (not expanded globally) medium, where all mass asymptotically tends to the cold phase. We also find that the development of a two-phase medium can be suppressed by a fast expan-

sion, when  $t_0/t_c < 10^2$ . The final mass fraction of the cold phase is larger for the slower expanded medium. Also, the final mass fraction depends on the amplitude of initial perturbations. Usually, the larger amplitude produces a larger final mass fraction of the cold phase. These results of the calculations are general with respect to the assumed geometry of perturbations. In the case of one-dimensional and periodical perturbations we compare them with the results of hydrodynamical calculations. We show that our statistical isobaric approach correctly describes the thermal instability process on the length scales up to  $\lambda \simeq \lambda_P$ . The hydrodynamical models show a weak dependence on the final mass fraction on the length scale in case of  $\lambda > \lambda_P$ .

The presence of a quite strongly tangled magnetic field of character length scale  $\lambda_m \ll \lambda_P$  can suppress the thermal instability, because the magnetic pressure will obstruct to the contraction of the cold phase. In the case of a large scale magnetic field  $\lambda_m \gtrsim \lambda_P$  the contraction of cold gas will occur mainly along magnetic strength lines forming thin and flat structures (see also Meerson & Sasorov 1987 and Sasorov 1988, where the formation of flattened plasma condensations was studied).

In the case of a large scale magnetic field  $\lambda_m \gtrsim \lambda_P$  the influence of the electron thermal conduction can be important. Our approach is valid in the limited time interval,  $t_0 < t < t_0 + \tau + t_\kappa$ , when the hot phase temperature is not too high,  $T_h < T_\kappa$ . At temperature  $T_h = T_\kappa$  the heating rate (5.2) of the hot phase is compensated by the cooling effect of the thermal conductivity  $\dot{T}_h = \kappa T_\kappa \mu / R \rho_h \lambda^2$ , where  $\kappa = a T^{5/2}$  is the coefficient of thermal conductivity (Spitzer 1962), and  $a = 10^{-6}$  in *cgs* units. In case of  $t_\kappa \ll t_0$  the estimation gives  $T_\kappa \simeq 3 \cdot 10^5 (\lambda/\lambda_P)^{4/7} K$ , and  $t_\kappa \simeq (T_\kappa/T_0) t_c \simeq 30 (\lambda/\lambda_P)^{4/7} t_c$ . At short scales  $\lambda \lesssim 10^{-2} \lambda_P$  the thermal conduction suppresses the thermal instability even in the linear stage (Field 1965). The perturbations of length  $\lambda \simeq \lambda_P$  can grow up to the maximum temperature  $\simeq 3 \cdot 10^5 K$ . Note that these estimations do not depend on the density and heating rate. The thermal conductivity facilitates the mass exchange between cold and hot phases. The following evolution of the two phases medium will be determined by this mass exchange process (see Aranson et al. 1993; Aharonson et al. 1994).

There is not a full understanding of the problem of dominate scales of perturbations resulting in the thermal instability process in the smooth scenario. It is known that the fastest growth rate has the modes with  $\lambda \lesssim \lambda_P$ . But, as it is shown earlier, the electron thermal conduction can suppress the growth of the shortest wavelength modes. On the other hand, the longer wavelength modes,  $\lambda > \lambda_P$ , have a slower development with an increase of the wavelength. Thus, there must be a dominate scale, which is determined by the competition of these factors. Another important factor, which has an influence on the value of the dominate scale, is the initial (at the moment  $t_0$  of the marginal stability) spectrum of perturbations. This spectrum depends on the past history of the medium. We can just note that the linear theory predicts the dumping of any perturbations at this stage,  $t < t_0$ , and that the shorter wavelength modes are dumped faster. Finally, it seems that the dominate scale will be located close to  $\lambda_P$  for a typical condition of the optically thin astrophysical plasma.

The possibility of the two-phase medium model for

quasars was first discussed by McCray (1979). The proposed expanding cloud scenario of thermal instability can be relevant to the formation of this two-phase medium, when warm ( $T \simeq 10^4 K$ ) clouds are formed as the result of thermal instability in an expanded gas fragment, which is a product of either a star-star collision (Spitzer & Saslaw 1966) or star-accretion disc collision in the  $\sim 1pc$  region around the quasar. The gas would be heated and ionized by the UV and X-ray emission of the quasar.

## ACKNOWLEDGMENTS

We thank for discussion G. Field, P. Goldreich, D. Kompaneets, R. McCray and I. Novikov. This research was partially supported by the Swedish Natural Science Research Council and by the Cariplo Foundation for Scientific Research. We would like to thank R. Turolla and A. Treves for support during our staying at the University of Padova and University of Milano, and R. Nicol and B. Högmán for improving the grammar of the text. The research of AFI was also supported by the grant RFBR 97-02-16975.

## REFERENCES

- Aharonson V., Regev O., Shaviv N., 1994, ApJ, 426, 621  
 Aranson I., Meerson B., Sasorov P.V., 1993, Phys. Rev. E, 47, 4337  
 Cox D.P., Tucker W.H., 1969, ApJ, 157, 1157  
 Elphick C., Regev O., Shaviv N., 1992, ApJ, 392, 106  
 Field D.F., 1965, ApJ, 111, 314  
 Krolik J.H., McKee C.F., Tarter C.B., 1981, ApJ, 249, 422  
 Lepp S., McCray R., Shull J.M., Woods D.T., Kallman T., 1985, ApJ, 288, 58  
 Meerson B.I., Sasorov P.V., 1987, Sov. Phys. - JETP, 65, 300  
 McCray R., 1979, in Active Galactic Nuclei, ed. C. R. Hazard and S. Mitton, Cambridge: Cambridge University Press, p. 227  
 McKee C.F., Begelman M.C., 1990, ApJ, 358, 392  
 Raymond J.C., Cox D.P., Smith B.W., 1976, ApJ, 204, 290  
 Samarskij A.A., Popov J.P., 1980, Differential methods for solving of gasdynamics problems, Moscow, Nauka, p.101 (in Russian)  
 Sasorov P.V., 1988, Sov. Astron. Lett., 14, 129  
 Spitzer L., 1962, Physics of Fully Ionized Gases. Interscience Publishers, New York, pp. 135, 145  
 Spitzer L., Saslaw W., 1966, ApJ, 143, 400  
 Weymann R., 1960, ApJ, 132, 452

## APPENDIX A: NUMERICAL METHOD

We briefly describe the numerical procedure to solve the equations (3.12) and (3.15) of the statistical approach. The equations are solved on the interval  $(T_{\min}, T_{\max})$  of definition of the distribution function  $\varphi(T)$ . The interval is divided on  $N$  subintervals by the grid points  $T_i$ , where  $i = 0, 1, \dots, N$ , and  $T_0 = T_{\min}$ ,  $T_N = T_{\max}$ . The evolution of each point  $T_i$  is defined by the equation (3.12). If the distribution of  $\{T_i^n\}$  are known at moment  $t^n$ , one can find the new values of  $\{T_i^{n+1}\}$  at moment  $t^{n+1}$  solving the system of algebraical equations

$$\frac{T_i^{n+1} - T_i^n}{\Delta t^n} = \frac{1}{2} (F_i^{n+1} + F_i^n), \quad i = 0, 1, \dots, N, \quad (A1)$$

where

$$F_i^k = -\frac{\gamma-1}{\gamma} \frac{\mu}{R} \left\{ \langle \rho \rangle^k \left( (\gamma-1) \left( \frac{\Lambda}{T} \right)^k T_i^k + \frac{\Lambda(T_i^k)}{T_i^k} \overline{T}^k \right) - H^k \left( (\gamma-1) \frac{T_i^k}{\overline{T}^k} + 1 \right) \right\} - (\gamma-1) \left( \frac{\dot{V}}{\overline{V}} \right)^k T_i^k,$$

$$\overline{T}^k = \sum_{i=0}^{N-1} \int_{T_i^k}^{T_{i+1}^k} \varphi^k(T) T dT,$$

$$\left( \frac{\Lambda}{T} \right)^k = \sum_{i=0}^{N-1} \int_{T_i^k}^{T_{i+1}^k} \varphi^k(T) \frac{\Lambda(T)}{T} dT.$$

Here  $\Delta t^n = t^{n+1} - t^n$  is the time step. The upper indices denote the corresponding time. The function  $\varphi^k(T)$  is piecewise-linear distributed through its average grid values  $\varphi_{i+1/2}^k = \Phi_{i+1/2}/(T_{i+1}^k - T_i^k)$ , where

$$\Phi_{i+1/2} = \int_{T_i}^{T_{i+1}} \varphi(T) dT, \quad i = 0, 1, \dots, N-1, \quad (A2)$$

are conserved quantities,  $\Phi_{i+1/2}(t) = \text{const}$ , as it follows from equation (3.15). The algebraical equations (A1) are solved by the Newton-Raphson method. The time step  $\Delta t^n$  and the number of iterations are determined by the assumed accuracy and convergency of the solution. Described numerical procedure can not be applied to calculate the evolution stage of highly inhomogeneous medium, when the time step becomes very small due to small differences  $T_{i+1} - T_i$ . In this case we modify the numerical algorithm introducing a grid redistribution procedure at each time step. Namely, we choose new values of  $\{T_i\}$  inside of the interval  $(T_{\min}, T_{\max})$  and remap  $\{\Phi_{i+1/2}\}$  from the old values to the new ones.

## APPENDIX B: LINEAR THEORY IN THE SMOOTH SCENARIO

The linear theory of thermal instability (see Weymann, 1960, Field, 1965) provides us the relations

$$\frac{P_1}{P_0} = -\alpha \frac{\rho_1}{\rho_0} = \frac{\alpha}{1+\alpha} \frac{T_1}{T_0}, \quad (B1)$$

where  $\alpha = \gamma(\lambda n / 2\pi c_s)^2 = \gamma \ell^2 x^2$ , between the perturbed pressure  $P_1$ , density  $\rho_1$  and temperature  $T_1$  with a wavelength  $\lambda = \ell \lambda_P$ , also the velocity variation  $v/c_s = ix \ell \rho_1 / \rho_0$ , and also the growth rate  $n = x/t_c$  of the condensation mode, where  $x$  is a positive real root of the equation

$$\ell^2 x^3 + \beta \ell^2 x^2 + x = x_0. \quad (B2)$$

Other two roots correspond to the damped wave modes. Here  $x_0 = n_0 t_c$ ,  $\beta = \gamma(\gamma-1)$ . The scale parameters  $\lambda_P$ ,  $t_c$  and  $n_0$  are given by equations (3.1), (3.2) and (3.17'), respectively. We supply here and below the index 0 to all relevant parameters (such as  $n$ ,  $N$ ,  $\tau$ ), which are used in the main text [see formulae (3.17'), (4.3)-(4.5)].

In a frame work of the smooth scenario (Section 4), when  $\xi = t_c/t_0 \ll 1$ , the parameter  $x_0(t)$  increases slowly and changes the sign from negative to positive at  $t = t_0$  linearly [equation (4.3)]

$$x_0(t) = a \frac{\delta t}{t_0}, \quad \delta t = t - t_0, \quad (B3)$$

where  $a = 3b(\gamma - 1)$ . In this scenario the linear theory at  $\delta t > 0$  gives the following:

1. The  $\ell = 0$  case corresponds to the isobaric S-model. We set  $\ell = 0$  into equations (B1) and (B2), and find  $\alpha = 0$  and the root  $x = x_0$ . The linear stage of the S-model is described by the equations (4.3)–(4.5) for the  $n_0 = x_0/t_c$ , the integral  $N_0(t)$ , and the end time  $\tau_0$ , respectively. The integral

$$N_0(t) = \frac{x_0^2(t)}{2a\xi} \quad (\text{B4})$$

reaches the  $N_0 = L_0 = \ln(1/A_0)$  level (when the amplitude  $A = A_0 e^{L_0} = 1$ ) at the end time

$$\tau_0 = X_0 \frac{t_0}{a} = \frac{t_0}{a} \sqrt{2aL_0\xi}, \quad (\text{B5})$$

when the end (maximal) growth rate reaches

$$X_0 = x_0(\tau_0) = \sqrt{2aL_0\xi}. \quad (\text{B6})$$

Note that  $x_0 \leq X_0 \sim \xi^{1/2} \ll 1$ , when  $\xi \ll 1$ .

2. The  $\ell > 0$  cases correspond to the hydrodynamical models ( $\ell = 1$  for the H1 and  $\ell = 5$  for the H2-models). The integral  $N_\ell$  has an implicit form now

$$N_\ell = \frac{1}{t_c} \int_0^{\delta t} x dt = \frac{x^2}{2a\xi} \left(1 + \frac{4}{3}\beta\ell^2 x + \frac{3}{2}\ell^2 x^2\right), \quad (\text{B7})$$

where we use  $dt = t_0 dx_0/a$  [see equation (B3)],  $dx_0/dx$  follows from equation (B2) and  $x$  is defined by equation (B2). The end rate  $X_\ell$  can be found from equation

$$2a\xi L_\ell = X_\ell^2 \left(1 + \frac{4}{3}\beta\ell^2 X_\ell + \frac{3}{2}\ell^2 X_\ell^2\right), \quad (\text{B7}')$$

which is followed from equation (B7) where we set the end value  $N_\ell = L_\ell = \ln(1/A_{0\ell})$ . Note, that  $X_\ell < \sqrt{2aL_\ell\xi} \sim \xi^{1/2} \ll 1$ . The end time  $\tau_\ell$  follows from equations (B2) and (B3),

$$\tau_\ell = \frac{t_0}{a} (X_\ell + \beta\ell^2 X_\ell^2 + \ell^2 X_\ell^3), \quad (\text{B8})$$

where  $X_\ell$  is taken from (B7').

3. It is useful to compare  $N_0$  and  $N_\ell$  [equations (B4) and (B7)], because the difference  $\Delta N = N_0(t) - N_\ell(t)$  determines the suppression of the hydrodynamics modes ( $\ell \neq 0$ ) relative to the isobaric mode ( $\ell = 0$ ). Substituting  $x_0$  from equation (B2) to (B4) we find the difference

$$\Delta N = \frac{\beta\ell^2}{3a\xi} x^3 g(x), \quad (\text{B9})$$

where  $x$  is determined by (B2) and

$$g(x) = 1 + \frac{3x}{4\beta} [1 + 2\ell^2(\beta + x)^2]. \quad (\text{B10})$$

It is also useful to compare the end times  $\tau_\ell$  and  $\tilde{\tau}_0 = \tau_0(L_\ell/L_0)^{1/2}$  [see equation (B5)], where  $\tilde{\tau}_0$  is the end time of  $\ell = 0$  mode when the initial amplitude of this mode is equal to  $A_{0\ell}$ . The end times difference can be obtained from the form

$$\tau_\ell^2 - \tilde{\tau}_0^2 = \frac{2}{3} \left(\frac{t_0}{a}\right)^2 \beta\ell^2 X_\ell^3 g(X_\ell), \quad (\text{B11})$$

where  $X_\ell$  is taken from equation (B7').

4. Note that in our case  $\xi \ll 1$ , when any  $x, x_0, X_0, X_\ell \sim \xi^{1/2} \ll 1$ , the terms  $x^2$  in the brackets in equations (B7) and (B7'), the terms  $x^3$  in equations (B2) and (B8), and the

**Table B1.** Parameters of the S-model ( $\ell = 0$ ), H1-model ( $\ell = 1$ ) and H2-model ( $\ell = 5$ ) followed from the linear theory.

$\ell$	$x(\tau_0)$	$N_\ell(\tau_0)$	$X_\ell$	$\tau_\ell/t_0$	$\alpha(X_\ell)$
0	0.063	10	0.063	0.0316	0
1	0.059	9.56	0.060	0.0323	0.006
5	0.033	6.0	0.040	0.042	0.067

$x$ -term in the bracket in equation (B10) can be omitted. The equation (B2) is a quadratic now:  $\beta\ell^2 x^2 + x = x_0(t)$  and has a root

$$x = x(t) = \left(\sqrt{1 + 4\beta\ell^2 x_0(t)} - 1\right) / 2\beta\ell^2. \quad (\text{B12})$$

Substituting  $x(t)$  in equations (B7) and (B9) we obtain the explicit time-dependencies of  $N_\ell(t)$  and  $\Delta N(t)$ . We also find  $\alpha(t)$  [see equation (B1)] and can now construct both the  $\sigma_T(t) = \sigma_0 e^{N(t)}$  and  $\sigma_P(t) = \alpha(t)\sigma_T(t)/(1 + \alpha(t))$  functions on the linear stage, at  $0 < \delta t < \tau_\ell$ . Graphs of these functions coincide well with the left-hand branches (at moments  $0 < \delta t < \tau_\ell$ ) of the corresponding lines in Fig. 5.

5. In the case  $\ell^2 x_0 \ll 1$  the above written formulae can be reduced to the simpler forms. From equations (B2, B12) we find

$$x \simeq x_0 - \beta\ell^2 x_0^2, \quad x < x_0 \ll \frac{1}{\ell^2}. \quad (\text{B13})$$

The difference (B9) in the main ( $x = x_0$ ) order is

$$\Delta N(t) \simeq \frac{\beta\ell^2}{3a\xi} x_0^3(t). \quad (\text{B14})$$

This difference at the end time  $\tau_0$  of the  $\ell = 0$  mode, when  $x_0 = X_0 = \sqrt{2aL_0\xi}$  [see equation (B6)], is

$$\Delta N(\tau_0) \simeq \frac{2}{3}\beta\ell^2 L_0 \sqrt{2aL_0\xi}. \quad (\text{B14}')$$

The end rate  $X_\ell$  can be found from equation (B7')

$$X_\ell \simeq \sqrt{2aL_\ell\xi} \left(1 - \frac{2}{3}\beta\ell^2 \sqrt{2aL_\ell\xi}\right). \quad (\text{B15})$$

The end time [equation (B8)] is now

$$\tau_\ell \simeq \frac{t_0}{a} \sqrt{2aL_\ell\xi} \left(1 + \frac{1}{3}\beta\ell^2 \sqrt{2aL_\ell\xi}\right), \quad (\text{B16})$$

and the end times difference [equation (B11)] is

$$\tau_\ell - \tilde{\tau}_0 \simeq \frac{2}{3}\beta\ell^2 L_\ell t_c. \quad (\text{B17})$$

6. For numerical examples we take  $b = 1$ ,  $\gamma = 5/3$ ,  $a = 2$ ,  $\beta = 10/9$ ,  $\xi = t_c/t_0 = 10^{-4}$ ,  $L_0 = L_\ell = 10$ . Results are shown in Table B1 and can be compared with the results of the statistical theory and exact hydrodynamical calculations presented in Section 5.

This paper has been produced using the Royal Astronomical Society/Blackwell Science L<sup>A</sup>T<sub>E</sub>X style file.